1

Deciphering Plasmonic Modality to Address Challenges in Disease Diagnostics

Esma Derin[1,2], Özgecan Erdem[1], and Fatih Inci[1,2]

[1]UNAM-National Nanotechnology Research Center, Bilkent University, Ankara, Turkey
[2]Institute of Materials Science and Nanotechnology, Bilkent University, Ankara, Turkey

1.1 Introduction

Recent advances in health technologies have remarkable impact on health-care system. Advanced health technologies are however not affordable and available for resource-constraint settings. From global health perspective, recent improvements in health technologies need to reflect alternative solutions for overcoming such inequalities by developing new technologies and strategies in the manners of cost-effective, rapid, easy-to-use, and portable size, hereby minimizing the disparities between resource-rich and limited settings [1, 2]. In this regard, biosensing arena has enormous applications in diverse fields, spanning from biomedicine to agriculture; for instance, monitoring vital information for diseases detection or determining the presence of contaminants in water and soil [2]. The concentrations of analytes can be accurately determined based on a linear association between signal intensity and analyte concentrations via an analytical biosensor. In the field, four types of biosensors, such as optical (mostly plasmonic sensors), electrochemical, piezoelectric, and magnetic biosensor, are mainly employed for analytical measurements [3]. Optical biosensors (e.g. surface plasmon resonance (SPR), localized SPR (LSPR), surface-enhanced Raman scattering (SERS), plasmon-enhanced fluorescence (PEF), surface-enhanced infrared absorption spectroscopy (SEIAS), etc.) are some of the mostly applied biosensors in health-care biomedicine [4, 5]. Especially, SPR-stemmed platforms have been benefitted in a vast majority of bio-analytical analyses since this technique enables rapid observation of bio-analytes in specimens, at the same time provides high sensitivity and selectivity in comparison to currently available instruments [2, 6]. These sensors basically monitor minute alterations in spectral properties of the plasmon by acting as a transducer of the sensing signal [5]. The sensing mechanism is constituted by recognizing and capturing the target analytes through bioreceptor which are immobilized on the metal surface. Then local refractive index increases due to capturing and SPR signals are shifted [7]. Their plasmonic fashion can be designed by considering the material and plasmonic features, like surface-based strategies that support SPP mode or nanoparticle-based

modality that employs localized surface plasmon resonance (LSPR). The intensity and peak position of the SPR have been influenced by the size, shape, and composition of the nanostructures and also the surrounding environment's dielectric properties. [5]. To touch upon the fundamentals of plasmonic sensors, they are stemmed from surface plasmon polariton (SPPs) or plasmonics, which are basically defined as the collective oscillations of free electrons at the metal surface [8]. Plasmonics deal with the electromagnetic (EM) wave and free electron interactions through excitation on conductors, such as metals, semimetals or semiconductors [9]. The excited electrons leads to collective oscillation with the close frequency to EM wave [9].

The history of SPP modality takes back more than a century, however, the improvements in the field have not accelerated until notable leaps in the nanotechnology (e.g. nanoscale fabrication techniques) to achieve appropriate sized structures for the further discoveries [10]. For instance, importantly note here, Kretschmann and Otto are two pioneers to create Surface Plasmon Resonance (SPR) through coupling strategies. Afterwards, SPR-based sensor was leveraged by Liedberg et al. through the antibody and antigen relations, which can be identified as a critical direction for biosensing platforms [11]. Today, SPR has been considered as one of the most powerful biosensing platforms, especially in analytical chemistry and medicine [7].

1.2 Surface Plasmon Polaritons

SP is the propagating light waves at the conductor surface via trapping due to interactions with free electrons [12]. Per these interactions, collective oscillations with light waves result in a resonance as a response of free electrons [12]. The formation of the SP is carried out by the resonant interactions of surface charge oscillations and electromagnetic field of light, and these interactions enhance the dominancy of SPs simultaneously [12]. The definition of the SPP can be simplified as an electromagnetic wave, and more specifically, it is transverse magnetic (TM)-polarized optical surface wave that propagates directly along a surface between dielectric and a metal surface (Figure 1.1a) [13, 14]. In addition, metal surfaces have crucial charge density wave, which constitutes SPPs with the combination with electromagnetic fields that are maximum at the interface on the contrast through both media since they are decreased exponentially [14]. The amplitude of the SPP is influenced inversely (exponential decay) with the distance of each medium from the interface [13]. In addition to the metal surface, SPPs can be obtained from different metal structures, such as thin films, stripes, differently sized and shaped nanoparticles or differently patterns (e.g. holes, slits, grooves, gaps, or corrugations, etc.) [14]. SPPs or plasmonics are mostly utilized by the fields of medical diagnostics, biosensing, spectroscopy, nanophotonic, imaging, or circuitry due to their substantial properties, including energy asymptotes in dispersion curves, resonances, field enhancement and localization, high surface and bulk sensitivities, and subwavelength confinements [8, 14]. Another point is that SPPs have subwavelength property and field confinement since their ability is overweighted to traditional optical elements (e.g. lenses, spatial light modulators) by considering ability to spatial field modulations at nanoscale [8]. Majorly, Maxwell equations between interface of conductor (e.g. metals) and a dielectric layer are crucial for the investigation of physical properties of SPPs [15].
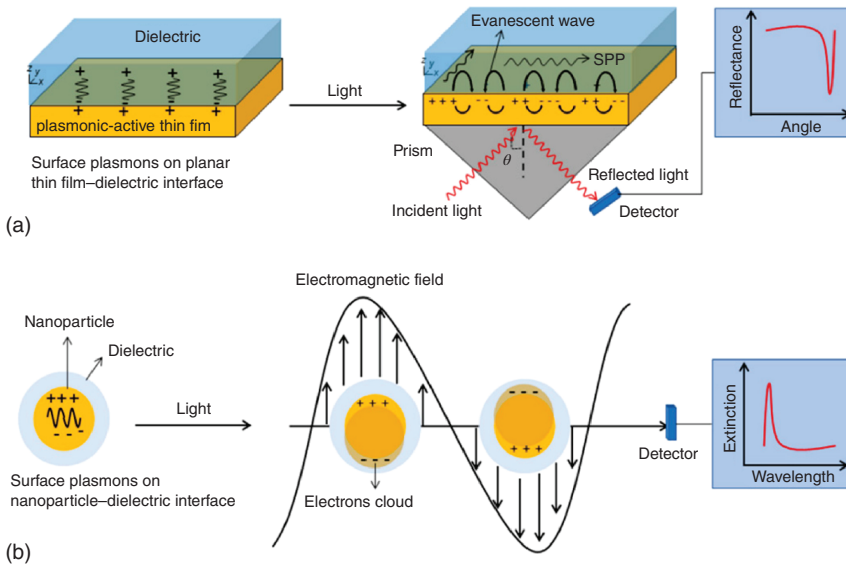
Figure 1.1 (a) SPP propagation is illustrated through thin film with the surface charges at the metal and dielectric interface with the excitation, and the spectra is obtained after surface plasmon excitation. (b) SPP is generated through nanoparticle surface to achieve localized surface plasmon resonance (LSPR), and the spectra is obtained after surface plasmon excitation. Source: Reprinted with permission from Bhattarai et al. [19]. © MDPI.

The characteristics of the SP modes, which can be either localized SPs of individual particles or several propagating SPPs on flat and curved, single and multiple surfaces, are determined by the topology of the metal surface. In addition, SPP modes of complex particle arrays and metal nanostructures are also determined. Based on this unique property of the SPP-based waveguides, the bandwidth of information can be transported by plasmonic waveguides through conventional (dielectric-based) photonics. The interest in plasmon-based nanophotonics is increased substantially [16]. When the SPP interacts with the metal, its energy dissipates. Free electron scattering in the metal, which is bounded with an ideal dielectric, creates loss due to absorption via inter-band transitions at a short enough wavelength [14]. For the SPP, this loss is fundamental. Operating wavelength selection can be selected carefully to avoid absorption via inter-band transitions or advanced fabrication techniques can decrease the free-electron scattering, and however, the both cannot be eliminated [14]. As aforementioned, surface of the metal interface has influence on the SPP, and moreover, the roughness creates additional loss since SPPs are scattered into bulk waves [14]. The main drawbacks of this loss are limiting practical applications of SPPs when it is excessive [14].

1.2.1 Excitation of the SPP

The excitation of the surface plasmon is mostly related to the conservation of the energy and momentum of photon in the incident light on a metal–dielectric interface. The excitation of the SPPs requires the momentum and energy matching to the incident photon's and plasmon
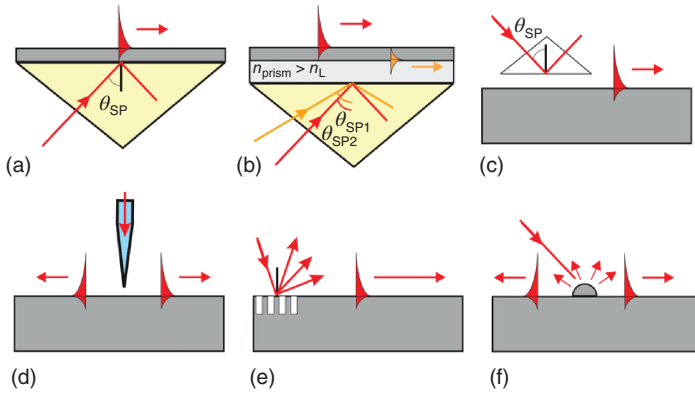
Figure 1.2 The common configuration of SPP excitations is depicted. (a) Kretschmann configuration, (b) two-layer Kretschmann configuration, (c) Otto configuration, (d) excitation with an SNOM probe, (e) grating diffraction, and (f) diffraction on surface features. Source: Reprinted with permission from Zayats et al. [24]. © 2005, Elsevier.

modes in order to obtain charge-coupled oscillations [17]. Special techniques are the primary requirement for the excitation of three-dimensional light beams in order to employ phase-matching [15]. The excitation of surface charges route can be explained by the presence of metal and dielectric interfaces and incoming p-polarized wave, which is transverse mode of the parallel electric field vector to the interface with an angle. The incident wave reaches the interface and split into two waves that are propagated in different directions [18].

Effective plasmon generation is achieved with the optical coupling element integration into the system. Prism, grating, and waveguide coupling methods (Figure 1.2) are the widely used light coupling techniques in comparison to waveguide, photonic crystal, and fiber-optic based coupling. These applications utilize attenuated total reflection (ATR), light diffraction or evanescent wave coupling from waveguide modes [17].

1.3 Surface Plasmon Resonance (SPR)

SPR is an optical biosensor that relies on the refractive index change of sensor surface, denoting label-free and in real-time detection [2, 20]. The plasmonics can be defined basically interaction of light with metals or metallic nanostructures; hence, this mechanism combines photonics and electronics to measure optical properties, e.g. spectra and refractive index changes at the nanoscale [3]. The interests in SPR biosensors have been increased enormously over the years [21]. The application of the SPR mostly focuses on clinical diagnostics, biological and pharmaceutical analysis, food quality and safety evaluation since it enables to monitor molecular interactions and quantify biomarkers, such as proteins, DNA or whole cells [22].

SPP or SP is the main requirement to induce SPR in the interface between the metal (e.g. gold or silver) and dielectric materials based on light excitation [22]. The generation of SPP in the form of EM wave occurs after the interactions of the incident light with metal since, collective oscillation of the free electrons is induced by the photons in the conduction band [23].

SPPs can be only sustained by p-polarized electromagnetic or transverse magnetic wave at an interface of metal and dielectric medium. The sign of the dielectric constant has to be opposite for instance gold, silver, copper, or aluminum, which have negative real and positive imaginary dielectric constants, and therefore, they can be used for the SPP generation [23]. These indicated metals have both pros and cons; for instance, the negative real dielectric constant of silver is the largest, which creates higher sensitivity against to refractive index (RI) changes. However, its chemical stability is lower due to easy oxidation in air. In contrast to silver, RI sensitivity of gold is lower, yet it holds higher stability and chemical versatility, and hence, the functionalization of the sensor surface can be carried out much easier.

1.4 Localized Surface Plasmon Resonance (LPSR)

Localized surface plasmon resonance (LSPR) is an optical phenomenon produced as a result of interactions between the incoming light and surface electrons in a conduction band through a light wave trapped in conductive nanoparticles smaller than the wavelength of light. This phenomenon is reliant on the size, geometry, dielectric environment, composition, and particle–particle separation distance of the nanoparticles [25]. Since metal nanostructures interact with a beam of light, some of the incoming photons are absorbed, and the rest are scattered in different directions. When LSPR is stimulated, these absorptions and scattering events increase greatly. In metal nanostructures, LSPR is most easily detected by an optical spectroscopic method, and this measurement is usually based on the extinction or scattering events [26]. The differences between SPR and LSPR are illustrated in Figure 1.3.

In addition to gold and silver, which are the most commonly used plasmonic materials, the other metals, such as copper [27] and aluminum [28, 29] also exhibit plasmon resonance features [30]. Mostly, the physical properties of metal particles change considerably when the size of particles is around nanoscale, and also, smaller than the wavelength of
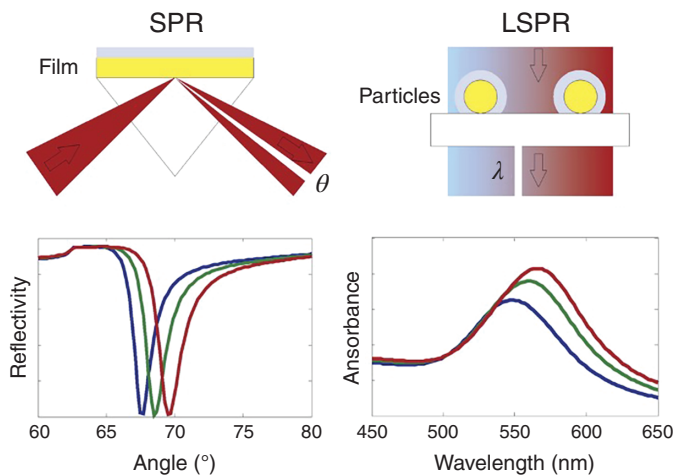

Figure 1.3 The schematic represents the basic principle and the difference between SPR and LSPR. Source: Reprinted with permission from Jatschka et al. [37]. © Elsevier.

light used to illuminate them [31]. In recent years, biosensors based on LSPR (majorly stemmed from metallic nanoparticles) have begun to draw attention for the label-free biosensing approaches due to its easy and colorimetric sensing features, as well as portability and its ability to interface with multiplexed devices [30, 31]. LSPR biosensors can also be easily integrated into miniaturized devices for point-of-care (POC) applications in order to save cost and reach the assay at different settings [32–34]. Integrating full-automation to these sensors also helps minimizing inter-personal errors for the measurements. Such integrations enable rapid acceleration for biosensor deployment into the health-care settings by promoting wider POC applications, such as bedside diagnosis, personalized medicine, and wearable devices [35]. Mostly, two main methods are used in LSPR biosensors: direct and indirect strategies. The first strategy tracks the shifts in the LSPR absorption peak due to the refractive index changes upon binding of the target molecule. This direct analysis requires less time and cost, but it has a limited sensitivity. The latter strategy is reliant on a sandwich analysis, where LSPR is used to stimulate the labels. As the light is on, metal nanostructures produce LSPR and are used to capture light near the surfaces [36].

On the other hand, there are also some obstacles. Since LSPR-based strategies are mostly dependent on the changes in the refractive index at the close vicinity of nanoparticles, a large number of molecules need to be localized around the particles in order to create a plasmonic shift. Strategies, such as adjusting the size and shape of the nanoparticle material, could be utilized to overcome this limit [30]. Another obstacle could be the reproducibility of sensor surface comprised of nanoparticles, ultimately limiting their utility and expansion to hurdle the real-world problems in clinical use.

From an application perspective, sensitive and selective detection of cancer biomarkers is of great importance in the early diagnosis of this disease. In a study, for instance, a LSPR lab-on-a-chip was designed to detect human alpha fetoprotein and prostate-specific antigen, which are cancer markers [38]. The microfluidic chip, which was developed by combining plasmonic, microfluidics, nanofabrication, and surface chemistry, accommodated 32 detection areas distributed across 8 independent microfluidic channels. The relevant markers could be detected quickly at a low concentration of $500\,pg\,ml^{-1}$ in a complex medium containing human serum, and the chip could be used multiple times. As another example, extracellular vesicles are abundant in various biological fluids, such as blood, saliva, urine, and extracellular matrix. Toxic signals derived from extracellular vesicles can spread on tissues adjacent to the damaged area in some diseases, including brain tumors and neurodegenerative disorders. In this regard, extracellular vesicles that can be used clinically for liquid biopsy, needs to be better characterized. An LSPR biosensor containing self-assembly gold nanoislands (SAM-AuNIs) was used to detect and differentiate SH-SY5Y from microvesicles isolated from A-549 cells [39]. Blood serum, lung cancer cell, and urine samples obtained from the mouse model were used as biological samples. Exosomes have been shown to produce a discernible response in the LSPR biosensor compared to microvesicles. According to these results, there was a different biophysical interaction between exosomes and microvesicles with SAM AuNIs.

In addition to their single-mode measurements, LSPR sensors can be integrated with different modalities. For instance, a dual-mode plasmonic biosensor that combines plasmonic photothermal effect and LSPR sensing transduction has been developed as a promising alternative method for the diagnosis of COVID-19 disease [40]. On this sensor, SARS-CoV-2-specific sequences can be detected precisely using 2D AuNIs functionalized

with complementary DNA receptors. When the thermoplasmonic heat was illuminated at the same AuNI chip at plasmonic resonance frequencies, a more sensitive sensing performance was provided.

1.5 Raman Spectroscopy and SERS

Raman spectroscopy is a method that measures the frequency shifts of the inelastic diffuse light from the sample when the photons hit a molecule and produce a diffused photon [41]. The photons of the laser light are absorbed successively by the sample, and the wavenumbers of re-sent photons are shifted up or down compared to the original monochrome waves (termed as the Raman effect). The resultant shift provides information about vibration, rotation, and other low wavelength transitions in molecules [42]. Near-IR (NIR), visible, or UV range monochromatic light is usually utilized for the Raman effect, which defines the photons to be adapted to virtual energy states, or energy stock generated due to the interaction of light with vibration modes associated with chemical bonds in the sample. Discrete vibration modes of the polarizable molecules are analyzed with such changes in energy, thereby obtaining a qualitative measurement of the biochemical composition [43]. Raman spectroscopy is a powerful analytical technique used in many areas, including detection of illegal drugs [44–46], toxic substances in the environment [47–49], and chemical [50–52] and biological warfare agents [53, 54], as well as *ex vivo* and *in vivo* applications of tissue diagnosis [55–58], and biomedical applications in which *in vitro* drug–cell interaction studies [59–62] are performed.

Resonance Raman effects that provide 10^2–10^6 enhancement, and Surface Enhanced Raman spectroscopy (SERS) resulting in up to 10^8 or both used together, which can provide up to 10^{16} enhancement, are used to increase the Raman signal [63]. SERS phenomenon is based on reduced Raman scattering when an analyte is adsorbed onto metal surface. The differences between SERS and Raman technique are represented in Figure 1.4. From the time when the discovery of the SERS, many researchers have begun to apply this method for molecular-level analysis, taking advantages of SERS, including high sensitivity, unique molecular fingerprint, and narrow spectral bandwidth for multiplex detection [64]. Known as an ultra-sensitive method that can detect even single molecules, SERS has long been considered a powerful tool, including the analysis of biomarkers that have been present in trace amounts. It offers an exceptional "signature" spectrum profile with very narrow peaks, capable of detecting multiple analytes simultaneously [65].
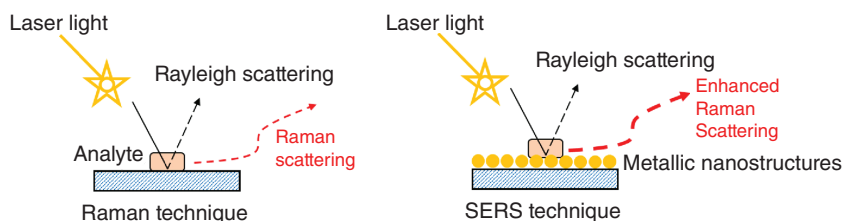

Figure 1.4 Basic principles of Raman and SERS technique. Source: Adapted and redrawn according to Zheng and He [66]. © John Wiley & Sons.

As a couple of examples in recent literature, a SERS sensor was fabricated using an Ag nanorod array by combining molecular signatures in the form of special hairpin to detect lung cancer-related miRNA biomarkers. With a portable-sized sensor, three different miRNAs (miRNA-21, miRNA-486 and miRNA-375) related to lung cancer were detected qualitatively and quantitatively [65]. As another example, a new paper-based, surface-enhanced SERS detection platform was developed to detect two key cytokines related to atherosclerosis, causing many cardiovascular and cerebrovascular diseases [67]. Two key cytokines, i.e., Interleukin 10 and monocyte chemoattractant protein 1, play key roles in the progression of this disease at different levels, and they are used for monitoring status and early diagnosis. A nanoporous networking membrane as a substrate and SERS nanotags as a signal reading probe were designed as a sandwich strategy, thereby enabling precise and specific identification of cytokine targets in human serum. In another study, ultrasonic surface-assisted SERS biosensor of the target-bound, acute myocardial infarction-related miRNA (miR-133a) was developed for the detection of disease-related biomarkers [68]. Bimetallic probes with high stability and a strong surface plasmon resonance effect were captured with a duplex connector to perform signal amplification after synthesis with a controllable silver and gold ratio through a galvanic replacement method. In this way, the target miR-133a could be detected in a wide linear range with high selectivity compared to other miRNAs expressed in human heart. The multiplex detection of biomarkers of Alzheimer's disease is of great importance for early diagnosis and personalized treatment of the disease. As the last example here, different Raman dye coded polyA aptamer–AuNPs conjugates were employed as SERS agents for simultaneous detection of Ap (1–42) oligomers and Tau protein [69]. Here, specific protein-aptamer binding mediated aggregation of AuNPs and the accompanying plasmonic coupling effect enabled to detect protein biomarkers within 15 minutes.

1.6 Whispering Gallery Mode (WGM)

Basically, WGM sensors are resonating micro- or nano-structures that provide high quality factors (Q). Where the changes in Q or shear resonance wavelength is used to evaluate surrounding milieu or binding events on the WGM resonator's surface. Optical WGMs are a family of electromagnetic modes built in a resonator with axial symmetry. WGMs create resonances at certain frequencies that depend on the geometry of the resonator, the refractive indices of both the resonator and the surrounding environment, and also the polarization of the modes [70]. WGM resonators can be fabricated in different morphologies with specific spectral properties, such as narrow line width, high stability, and adjustability [71].

WGM-based sensors have been used to detect biological molecules; for instance, a platform monitoring the shifts in the WGM resonance frequency were fabricated to measure enzymatic oxidation of glucose (Figure 1.5) [72]. The platform was modified with glucose oxidase and gold nanoparticles. Throughout the enzymatic reaction catalyzed by glucose oxidase, electrons were transferred to gold nanoparticles, and the optical signals produced
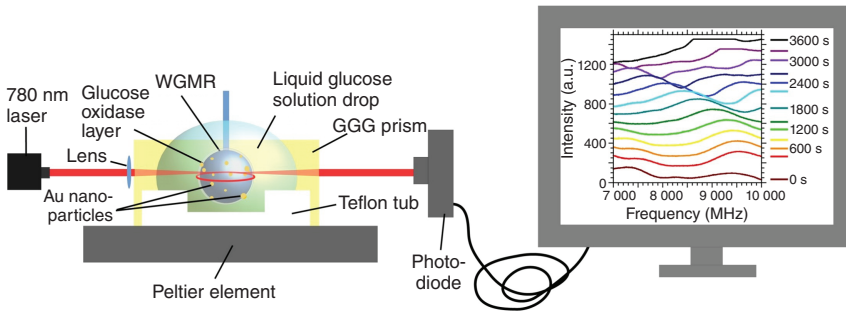
Figure 1.5 Schematic representation of WGM-based glucose sensor. Source: Reprinted with permission from Brice et al. [72]. © 2020, Elsevier.

by WGM resonators consisting of standard telecommunication fiber optics dissolved in a hydrogen flame were evaluated. As a result of tests that were performed at various glucose concentrations, the WGM-resonance frequency shift rate increased significantly at higher glucose concentrations.

In another study, a WGM resonator-based on fluorescence imaging has been reported to detect CA-125, i.e., an ovarian cancer biomarker [73]. Measurements have been extended using a simplified approach to initiate WGM resonances through excitation light coupled with the Dove prism. The mod structure in each resonator emerges thanks to the improved phase matching, thereby providing significant improvements in signal-to-noise. In addition, fluorescence imaging of the WGM resonances enabled for repeatable detection of biomarkers in complex biological fluids.

1.7 Fiber Cables Sensors

In recent years, the applications of fiber optic sensors in modern medical technologies and devices have been leveraged. Since the first generation of probes for *in vivo* pressure detection has been commercialized, the research is underway to develop new generation of fiber optic systems that have been significantly improved over the other sensing technologies, such as micro- and nanoelectromechanical systems [74]. Usually, a fiber optic probe is functionalized using biorecognition elements that can be selectively linked with target molecules. In the system, the response occurs based on a change in the local refractive index caused by the target. The biorecognition elements generally include various protein and nucleic acid-based molecules. The label-free detection methods using optical fibers enable to reach very low target detection limits. Gold, silver, magnetic nanoparticles and nanostructures with different shapes and sizes can be used as energy concentrators to expand the detection limits of optical fibers and obtain high-precision biosensing probes [75]. Fiber optic biosensors reliant on SPR [76–78], long-period grating [79–81] and fiber Bragg grating have been employed in a variety of fields and they provide rapid and precise detection [82].

As an example, fiber optic-based SPR type platform was utilized to detect acetylcholine, a pivotal neurotransmitter involved in the regulation of behavioral activities in human [83]. Dysfunction in acetylcholine regulation, for instance, has been linked to a variety of neurological disorders, including Alzheimer's disease. In this study, the sensing probe consisted of multiple layers of silver metal and tantalum-v-oxide nanoflakes functionalized with acetylcholinesterase on the uncoated core of an optical fiber. Once the sensing probe was exposed to acetylcholine solutions, the RI changed, and accordingly, the sensor provided a detection limit down to 38 nM of acetylcholine. In another study, a black phosphorus fiber optic biosensor was developed for the ultrasensitive detection of human neuron-specific enolase (a cancer biomarker) [84]. Biofunctionalized black phosphorus nanosheets by poly-L-lysine were exploited by integrating them into a largely curved fiber grid. After the nanosheets were synthesized by a liquid ultrasonication exfoliation, they were deposited on the fiber device by a layer-by-layer method. The anti-NSE immobilized BP-TFG biosensor was able to detect small cell lung cancer with a detection limit of $1.0\,\mathrm{pg\,ml^{-1}}$. A new non-invasive measuring probe based on the fiber Bragg grid (FBG) was designed as a hybrid multi-channel fiber optic sensor system [85]. The probe specifically monitored body temperature, breathing rate, and heart rate, and it was capable of processing signals coming up to 128 people continuously (Figure 1.6).
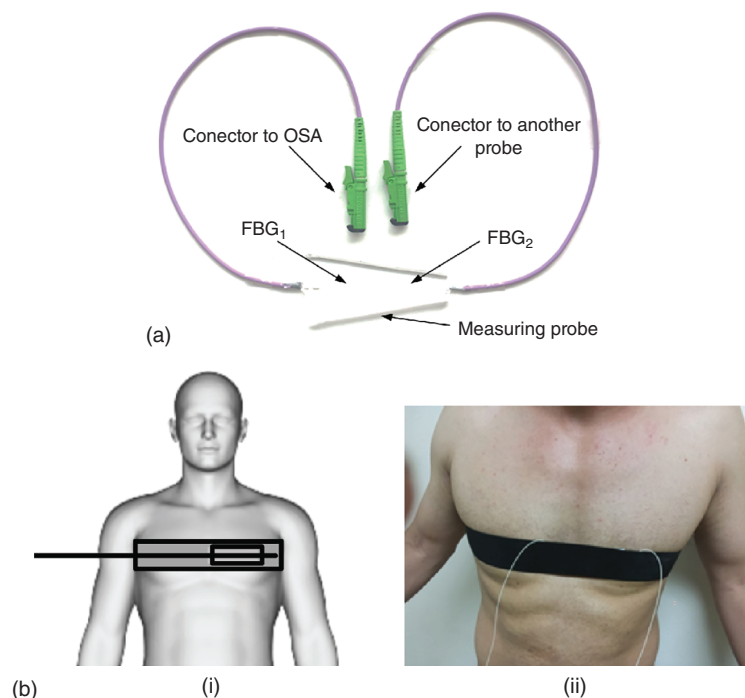

Figure 1.6 (a) The fiber-optic probe. (b) (i) A schematic diagram of the experimental set up. (ii) Experimental set up to acquire vital signals from a human subject using the probe embedded in a thoracic elastic strap. Source: Reprinted with permission from Fajkus et al. [85]. © MDPI.

1.8 New Trends in Plasmonic Sensors for the Applications in Disease Diagnosis

1.8.1 Mobile Phone-Integrated Platforms

The utilization of mobile phones in daily life mediates substantial opportunity for biomedical applications as a mobile device, potentially accelerating to reach health-care. The unique properties of the mobile phones (e.g., powerful CPUs, touch screen displays, advanced connectivity, high pixel-count, sensitive cameras, and integrated light sources) leverage their applicability to the biosensor realm [86]. These features also enable applications at resource-constrained settings, where the dedicated instruments and laboratory conditions do not exist [87]. As a consequence, integrating mobile phones with optical detection platforms creates a crucial niche that has evolved rapidly and denoted diverse biosensing approaches in the fields of immunodiagnostic assays, lateral flow assays, microscopic imaging, flow cytometry, colorimetric detection, photonic crystal, and SPR [86]. Talking over the examples, an enzyme-mediated LSPR strategy was employed to measure the RI changes around gold nanorods (AuNRs) while interacting with serum myoglobin, i.e., a biomarker for acute myocardial infarction (AIM) [88]. To eliminate complex readout systems, smartphone was turned into plasmonic immunoassay reader, which was designed as an ambient light sensor (ALS), and measured transmitted light intensity of AuNRs. The synthesis of AuNRs was carried out through the preparation of the seeded gold, which was used to create a sandwich immunoassay while exhibiting plasmonic properties [88]. The sensing strategy was based on hydrogen peroxide (H_2O_2) generation from glucose and gluconic acid catalysis since H_2O_2 caused a blue shift in the SPR spectrum of AuNRs. Then, blue shift was positively correlated with the target concentrations. Two pieces of the reader were 3D-printed, one of them fixed on a smart phone to supply a stable light source powered by two batteries, and the other one provided a host to microwells (Figure 1.7) [88]. The linear detection range of this
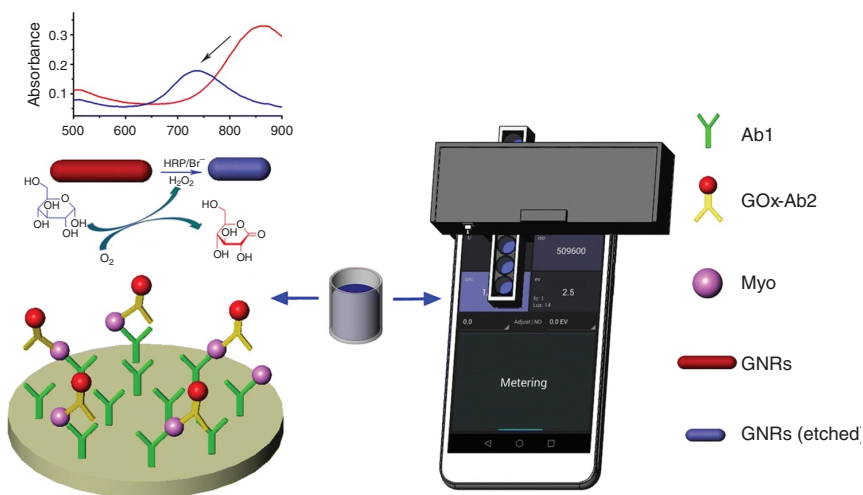

Figure 1.7 Schematic illustration of the AuNR-based plasmonic immunoassay for Myo detection. Source: Reprinted with permission from Yang et al. [88]. © Springer Nature.

platform was 0.1–1000 ng ml^{-1}, and LOD value for myoglobin detection was 0.057 ng ml^{-1}. This platform has presented high potential for biomedical applications due to higher sensitivity in comparison to conventional ELISA. Simply to put smartphone-based plasmonic immunoassay reader has enabled an easy access when the sources are limited [88].

1.8.2 Smart Material Integration

Recent studies have introduced micro/nano-size photonic/plasmonic structures, including photonic crystals (PC) or SPR-based metal nanostructures [89]. The PCs have ability to manipulate light in nontraditional ways because of photonic band structure concepts [90]. These structures are periodic arrangements of dielectric materials that interact with the light to provide reflection at specific wavelengths [91, 92]. The structure of PCs can be formed naturally or created rationally using different fabrication methods [91, 92]. In nature, well-known examples are present, such as *Morpho rhetenor* butterfly peacock, *Eupholus magnificus* insect, sea mouse, and opal. In an artificial way, PC structures can be fabricated in different dimensions (e.g., 1D, 2D, or 3D) with diverse materials including silicon, glass, polymers, colloids, and silk [91]. Among them, the unique and crucial properties (e.g., optical transparency, mechanical robustness, biocompatiblity, biodegradability, and facile functionalization) of silk fibroin provide important developments in photonics and biomedical device application [93]. One of the recent studies introduced robust, freestanding, 3D, PC fabrication in the form of inverse opal by using silk fibroin and created different lattice constants [94]. The methodology can be simply defined as a template that was constituted via placing differently sized (PMMA) submicrometric spheres on silicon substrate in the face-centered cubic (fcc) conformation and pouring silk fibroin extract. After solidifying of the silk solution, silicon substrate was detached; immersed in acetone to dissolve the PMMA spheres; and finally, amorphous free-standing inverse silk opal structure were obtained [94]. Moreover, as an example of hybrid PC-plasmonic platform, a recent study demonstrated an assay approach that was integrating plasmonic nanoparticle tags, imaging-based optical biosensor, and microfluidic device [95]. The integration of the microfluidic device reduced the assay time for the binding analytes to the biorecognition elements through diffusion. In this study, PC behaved as an active transducer for rapid imaging. Plasmonic AuNP created high-contrast digital resolution sensing of analytes on the LSPR spectra by overlapping with the resonance reflection of the PC [95]. AuNPs and immobilized PC were conjugated with antibodies that have an affinity to target analytes. When the AuNP-antibody conjugates capture HIV-1 capsid antigen (target analyte), they were applied through a microfluidic device, antibodies that are immobilized on PC captured AuNP-HIV-1 conjugates. [95]. The design of the sensing system utilized an absorbing paper pad to control single-pass flow rate. The assay was completed within 35 minutes, and LOD value was 1 pg ml^{-1}. This approach would be applied as a POC device for infectious disease diagnostics and early stage disease monitoring by the virtue of ultrasensitive and ultrafast biomolecule detection [95].

A recent study focused on to create an imaging-based plasmonic biosensor combining AuNPs and gold nanohole arrays (AuNHAs) in order to achieve highly sensitive detection of human C-reactive protein (CRP) for acute inflammatory diseases [96]. The detection principle integrates a heat-map generation based on the single NPs position. The

capture antibodies, which were immobilized in AuNHAs, reacted with the target bio-markers and second antibody that was immobilized on the NPs to recognize the bio-marker (Figure 1.8a), hence sandwich assay approach was achieved. After the binding, AuNPs created intensity dips (i.e., red spots) on a captured image due to strong local suppression in the transmission (Figure 1.8b). CRP could be detected as low as 27 pg ml^{-1} and this enabled to reach to the clinically relevant concentrations at four orders of magnitude. Single NP-labeled proteins could also detected via the digital quantification and localization of individual AuNPs.

Moreover, combining SPR strategy with NPs provides notable improvements in sensing manners [97]. In particular, optical, chemical, electronic, and catalytic properties of colloidal plasmonic nanoparticles (PNPs) have created paramount interest in plasmonics, sensing, catalysis, biomedical imaging, diagnostics, and therapeutics [98]. The applications of AuNPs are highly overweighted while comparing them with the other PNPs in the biomedical applications owing to chemical/biological inertness and low cytotoxicity, versatile, and straightforward surface functionalization (e.g., oligonucleotides, proteins, or antibodies) [98]. On the other hand, signal enhancement is crucial approach for biosensors as demonstrated in recent studies. For instance, a plasmonic patch, which was fabricated through absorbing plasmonic nanoparticles (different shapes were also investigated) into PDMS elastomer, was introduced to enhance the signal (Figure 1.9) [99]. The idea behind this fluorescence enhancement technique was to add a plasmonic patch onto diverse fluorescent surfaces in order to enable large and uniform fluorescence enhancement. In contrast to conventional plasmon enhancement techniques, this system does not require any protocol modification [99]. The mechanism of the enhancement was occurred via close proximity of the elastomeric film and fluorescent species on the surface. The enhancement of fluorescence was reached 100 times higher with the ~300-fold increase in the sensitivity due to the enhanced electromagnetic field. The sensing platform was applied with the acute kidney injury markers (e.g., KIM-1 and NGAL) to indicate diagnostic capability from urine samples [99].

As another example, the periodic patterns of the optical discs (e.g., compact discs [CDs], digital versatile discs [DVDs], and Blu-ray discs), which are commercially available, enable inexpensive (0.90–$1.50) and large area of active sensing for ultrasensitive biosensing applications [100, 101]. Their production scale is high to compensate for the demand in the market besides their potential usage for plasmonic biosensors. The quality of the optical discs has been evolved with time in terms of molding processes to obtain nanometer precision for their encoded structure [101]. Optical discs have been combined with several kinds of plasmonic sensor approaches, including SPR [100], LSPR [102], and SERS [101]. One of the recent studies demonstrated the detection of HIV-1 particles on a plasmonic metasurface DVD, exciting plasmonic Fano resonance modes to increase sensitivity for both multimodal and multiplex sensing. In this study, two or more molecular oscillations and small perturbation interferences created large spectral shifts in the resonance frequency as a response [103]. With the use of inherent periodic arrays of DVDs, the requirements of metasurface fabrication were remarkably reduced in terms of cost, time, and personnel efforts, compared to the conventional techniques, which have complex, lengthy, and highly expensive procedures. Overall, plastic-templated metasurfaces hold great potential for various applications (e.g., biochemical sensing, optoelectronics, and optical spectroscopy devices), and they
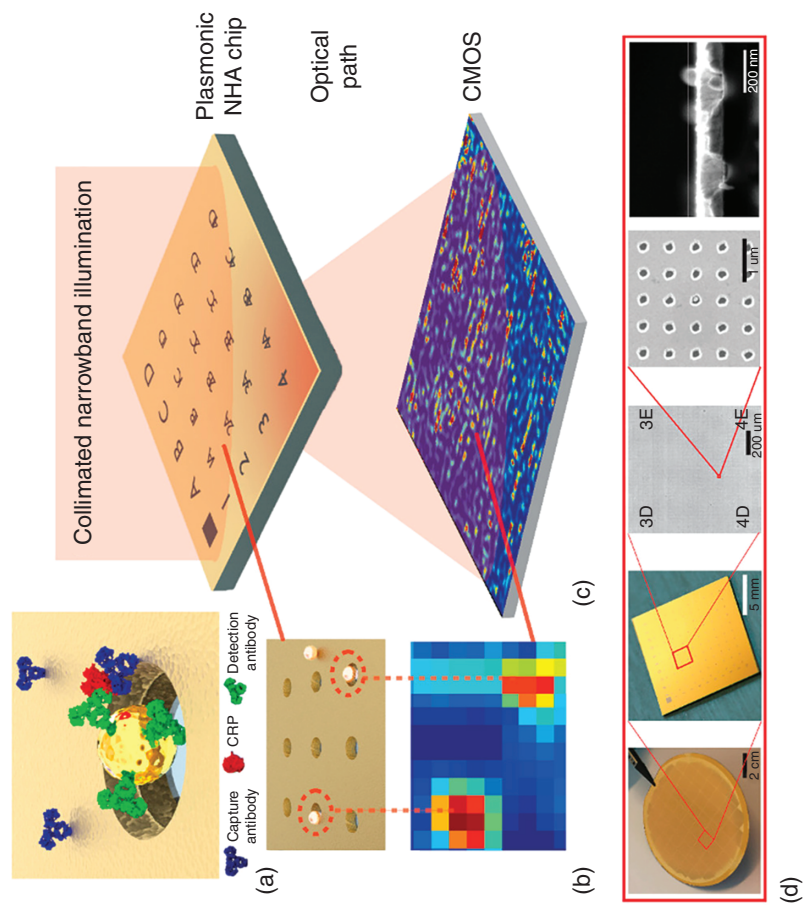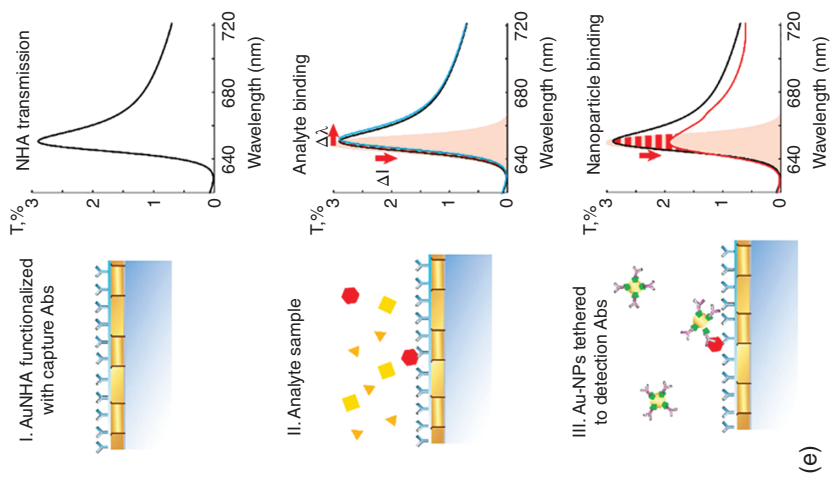
Figure 1.8 CRP detection via AuNP-enhanced plasmonic imager. (a) The schematic represents the capture of CRP (red) by an antibody (blue) on AuNHA and the detection of CRP by detection antibodies (green) tethered to AuNPs, respectively. (b) AuNPs create intensity dips (i.e. red spots) on captured image due to strong local suppression in the transmission. (c) Array labeling for accurate image processing and heatmap generation via CMOS camera for digital detection. (d) AuNHA wafer with 50 sensors. The plasmonic sensor surface is covered with AuNHAs. An image of microarray labels after patterning. The image of nanoholes ($D = 200$ nm, $P = 600$ nm) and the image of the nanohole containing AuNP are represented in the order from left to right. (e) (i) Transmission spectrum of the AuNHAs. (ii) peak position shift after the analyte binding, and (iii) local suppression after the binding of AuNPs to the AuNHA surface. Source: Reprinted with permission from Belushkin et al. [96]. © 2018, American Chemical Society.
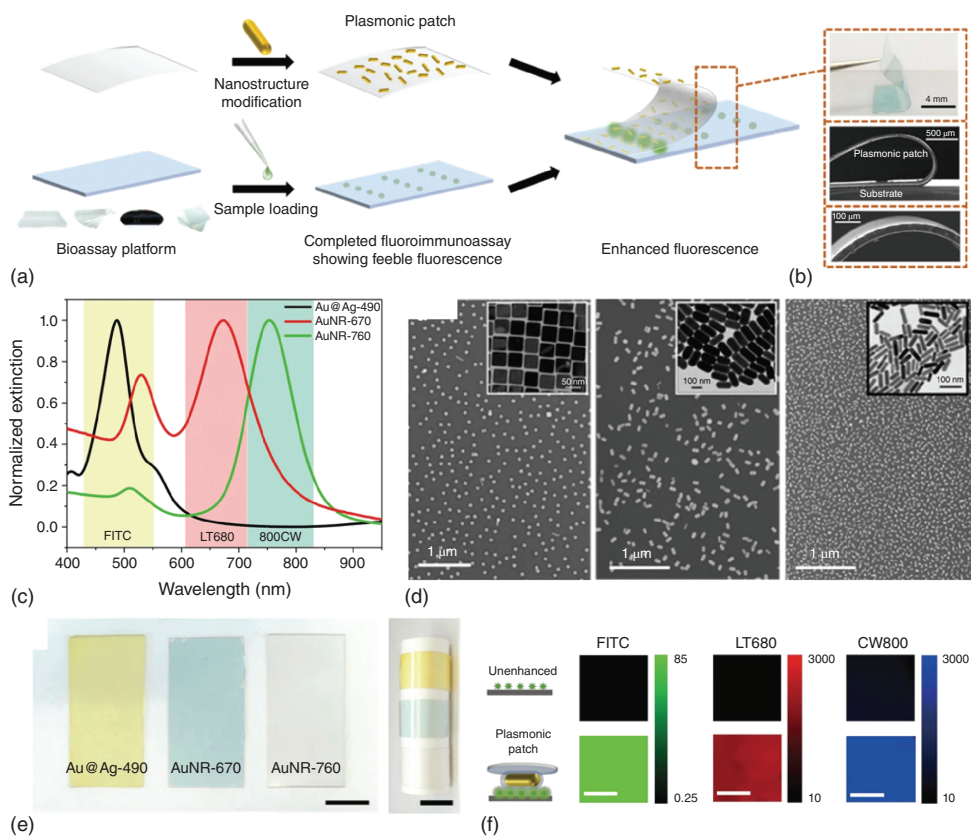
Figure 1.9 (a) The diagram of the plasmonic patch fabrication and application procedure for fluoroimmunoassays. (b) The image of the plasmonic patch transfer to assay surface, and an SEM image of the patch and its properties (e.g. thickness as 30 μm, flexibility, conformability). (c) Normalized extinction spectra of aqueous solutions for the differently shaped plasmonic nanostructures. (d) Characterization of the differently shaped AuNPs via an SEM imaging of plasmonic patch surface to demonstrate uniform distribution. (e) The patch image after modification with differently shaped nanostructures (scale bar represents 1 cm). (F) The fluorescence map of three fluorophores that were absorbed onto silicon wafer in the presence of plasmonic patch (the scale bar on green represents 10 μm; and the scale bar on red and blue represents 1 mm). Source: Reprinted with permission from Luan et al. [99].© Springer Nature.

present portability, cost-effectivity, and disposability properties [103]. In addition, plasmonic grating structures were utilized to estimate the thicknesses of biolayers formed on a plasmonic sensor by measuring entangled Fabry–Perot cavities (EFPC), leading to dual-mode sensing (SPP and LSPP) in order to eliminate background RI variations (Figure 1.10) [102]. This work was also applied to measure the size of exosomes, which is the useful information for neurodegenerative and cardiovascular disorders, and cancer. From the assay cost perspective, the fabrication was established by a large-area photolithography instead of e-beam lithography, and portable spectrometer was adapted to visible wavelengths, minimizing the need for complex and expensive instrumentation and setup.
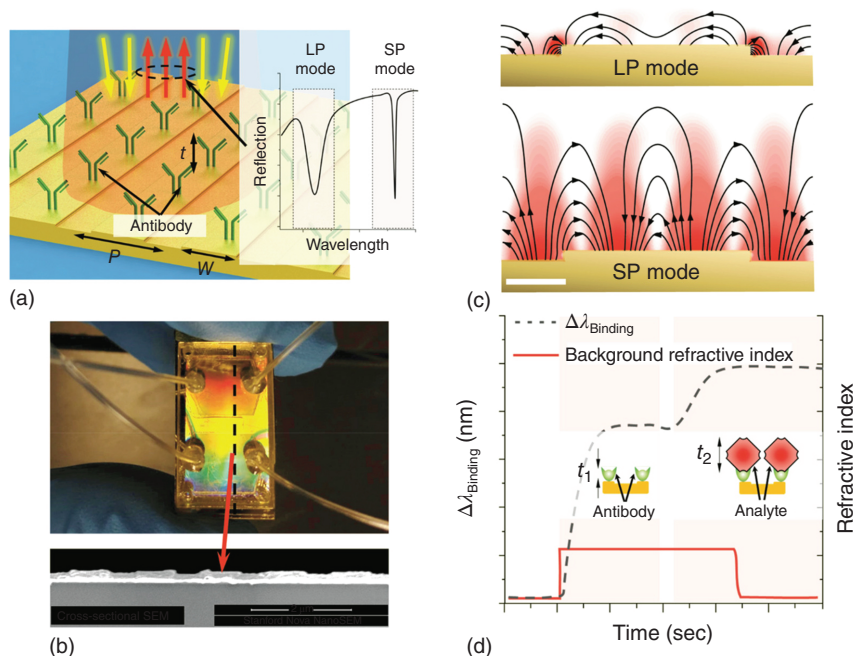
Figure 1.10 Schematic represents the working principle of plasmonic Fabry–Perot cavities. (a) The schematic illustrates the surface after the immobilization of antibodies to capture cellular entities and a typical reflection spectrum is depicted. (b) The image of the two-channel microfluidic chip, and an SEM image shows the cross-section of the sensor. (c) SPP and LSPP electric field distribution and field lines are demonstrated (scale bar 200 nm). (d) The typical data after multistep detection is presented and the data indicates the resonance shift data with respect to surface layer formation, bulk RI value, and the thickness of formed layers on the sensor surface. Source: Reprinted with permission from Mataji-Kojouri et al. [102]. © 2020, American Chemical Society.

1.8.3 Naked-Eye Detection

Technological advancements in the platforms-based on naked-eye detection are increasing promptly in the fields of health, environmental chemistry, food and beverage, bio-defense, and fermentation industry. Colorimetric sensors are important tools in diagnosing of various diseases, such as diabetes, cancer, Alzheimer, Parkinson, bacterial infections, depression, and infertility. These devices offer advantages as a real-time, high-precision, specific, and cost-effective alternative that are capable of analyzing results with naked-eye, simple integration with smartphones or color detection devices for the quantitative results [104]. A visually distinguishable color change is observed in the instant detection of the analyte on a colorimetric sensor. Metallic nanoparticles, such as Au, Ag, Cu, are widely employed in visual detection due to their optical properties [105]. Plasmonic colorimetric diagnostic platforms are the most suitable methods deployed into POC diagnosis. As a detection platform, their effortlessness in producing a signal output based on color change is advantageous [32]. The main theme in colorimetric sensors is how to transform the interactions of complex stimuli, such as molecule, temperature, pH value into visible color changes that can be seen by the naked-eye [106]. Smart-phones can be integrated with biosensors to develop POC devices that the end user can

use at remote settings easily. Along with the technological developments, camera quality on smart phones have been updated, and nowadays, they are one of the perfect tools for optical detection through monitoring the primary color bands, namely red, green, and blue [107].

Paper-based lateral flow assays (LFA) have been largely utilized in this regard. Typically, biomolecules, such as labeled antibodies are used to capture and detect a biomolecule through colorimetric or fluorescence reading. At the end of the test period, a color band is analyzed for qualitative and quantitative reading [108]. An example of interest in LFAs was implemented on a paper or nitrocellulose membrane [109]. The filtered solution then migrated to the conjugate pad through capillary forces, where tracers were released, such as the gold nanoparticle conjugated with the receptor. As another example, aptamer-based LFA was designed for rapid detection of cortisol in sweat, an important parameter to monitor physiological stress [110]. For this purpose, cortisol-specific aptamers were conjugated to AuNPs. In the presence of cortisol molecules, they interacted with the aptamer–AuNP complex and they were desorbed from the surface of AuNPs. Free gold nanoparticles were then captured by a reaction with the immobilized cysteamine in the test region of the LFA strip. Thus, cortisol was visually perceived within minutes. Figure 1.11 details the colorimetric
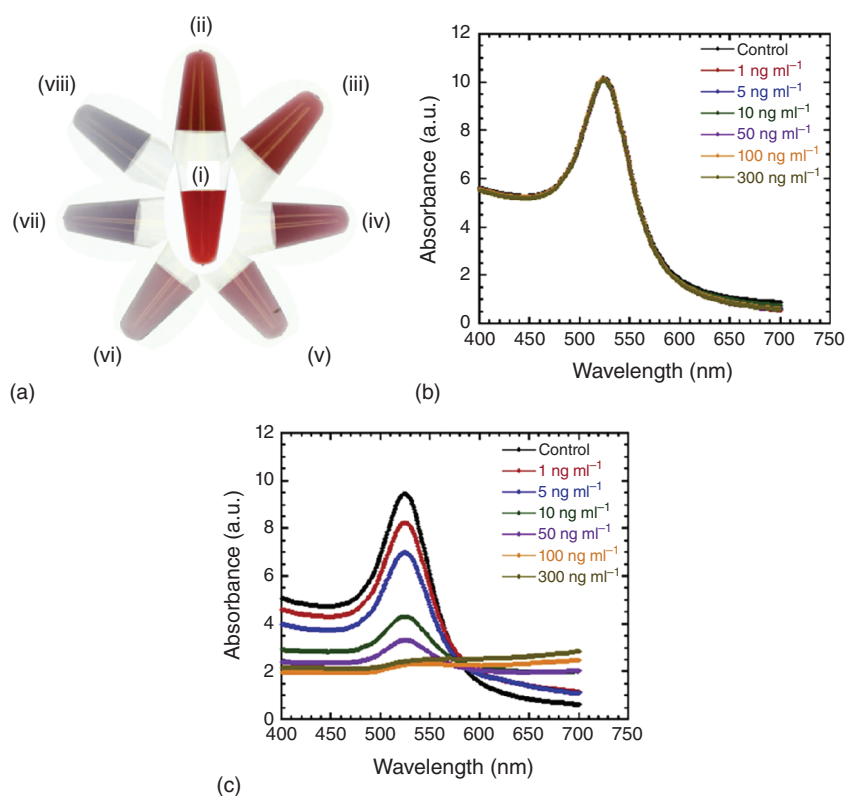

Figure 1.11 (a) Colorimetric detection of cortisol in artificial sweat (ii–viii:0–300 ng ml^{-1}). Optical spectra of mixture of DNA-AuNP and artificial sweat solutions with various cortisol concentrations: (b) without NaCl; (c) with NaCl. Source: Reprinted with permission from Dalirirad and Steckl [110]. © 2019, Elsevier.

detection of cortisol in artificial sweat. As another application, quantum dots (QDs) were integrated with an LFA to detect glutathione, which is a biothiol abundant in cells and plays a key role in many biological processes [111]. Herein, QDs- functionalized with bovine serum albumin were modified as signal reporter on the test line. When a binding occurs between Ag^+ and the QDs, the fluorescence level was effectively extinguished by electron transfer from QDs to Ag^+. In the presence of glutathione, Ag^+ preferred to react with glutathione by forming an Ag^+-S bond due to its stronger affinity. As a result, glutathione measurement was provided efficaciously using the fluorescence of the quantum dots. Furthermore, a fluorescent and colorimetric method was developed for multiplexed monitoring of cancer cells using graphene oxide-based aptameric nanosensors in microfluidic paper analytical devices [112]. Mesoporous silica nanoparticles-coated with quantum dots labeled as aptamers in a flexible single-stranded state was adsorbed on the graphene oxide surface. Here, three different cancer cells were identified simultaneously with a single excitation light, and the changes in colors were easily observed with the naked-eye.

1.9 Outcomes and Conclusion

In this chapter, we summarize the fundamentals of plasmonic modalities along with their applications in disease diagnostics. On the course of dramatic transition of biosensors from laboratory-based diagnostic assays to POC devices, there are important assets needed to be revisited before their implementation to the clinical settings, which include portability, cost, short assay time, less equipment need, quantitative results, acceptable LOD levels, reliability, and easy-to-use to the end-user, especially for an untrained personnel [95]. Especially, the rare number/level of biotargets is still an obstacle, guiding researchers to develop highly sensitive plasmonic tools [95, 113]. Considering the adaptation of plasmonic sensing to the POC settings, sensitivity could be improved via different strategies: (i) sensing based on target-induced local refractive index changes, (ii) colorimetric sensing based on LSPR coupling, and (iii) amplification of detection sensitivity based on nanoparticle growth [113]. As elaborated above, a variety of approaches, using large-area periodic nano-array patterns, such as nanosphere array, nano-disc array, or nano-triangle array instead of planar metal film would further improve refractive sensitivity since they support both a stronger local EM field and higher sensing area [5]. Furthermore, coupling plasmonic nanoparticles with Au films in the sandwich form would enhance the SPR shifts, compared to the measurements on a single Au film [5]. Inherent periodic arrays on plastic templates and low-cost fabrication techniques enable to fabricate sensitive plasmonic metasurfaces for not only monitoring the presence of biotargets, and also, measuring their sizes to help in biological investigations for research and clinical use.

In summary, plasmonic modality is a powerful technique capable of measuring nano-sized biological entities from biospecimens. With further developments described above and also with others such as integrating antifouling strategies, their sensitivity and reliability fashions would be improved remarkably. Although algorithms reliant on Artificial Intelligence and Machine Learning have not been elaborated here, plasmonic sensors would further benefit from these approaches, especially in terms of signal processing, accelerating assay time, and analysis for their proper utilization in the POC settings.

References

1 Howitt, P., Darzi, A., Yang, G.Z. et al. (2012). *The Lancet* 380 (9840): 507–535.

2 Firdous, S., Anwar, S., and Rafya, R. (2018). *Laser Physics Letters* 15 (6): 29–34.

3 Liu, J., Jalali, M., Mahshid, S., and Wachsmann-Hogiu, S. (2020). *The Analyst* 145 (2): 364–384.

4 Damborský, P., Švitel, J., and Katrlík, J. (2016). *Essays in Biochemistry* 60 (1): 91–100.

5 Li, M., Cushing, S.K., and Wu, N. (2015). *The Analyst* 140 (2): 386–406.

6 Inci, F., Celik, U., Turken, B. et al. (2015). *Biochemistry and Biophysics Reports* 2: 115–122.

7 Guo, X. (2012). *Journal of Biophotonics* 5 (7): 483–501.

8 Li, L. (2013). *Manipulation of Near Field Propagation and Far Field Radiation of Surface Plasmon Polariton*. Springer.

9 Nickelson, L. (2019). *Electromagnetic Theory and Plasmonics for Engineers*. Springer.

10 Barnes, W.L. (2006). *Journal of Optics A: Pure and Applied Optics* 8: 4.

11 Han, X., Liu, K., and Sun, C. (2019). *Materials* 12: 9.

12 Barnes, W.L., Dereux, A., and Ebbesen, T.W. (2003). *Nature* 424 (6950): 824–830.

13 Maradudin, A.A. (2014). *Modern Plasmonics*, vol. 4. Elsevier B.V.

14 Berini, P. and De Leon, I. (2012). *Nature Photonics* 6 (1): 16–24.

15 A. S.Maier, Plasmonics: Fundamentals and Applicaitons 2007.

16 Han, Z. and Bozhevolnyi, S.I. (2014). *Modern Plasmonics*, vol. 4. Elsevier B.V.

17 Tokel, O., Inci, F., and Demirci, U. (2014). *Chemical Reviews*.

18 Zhang, J., Zhang, L., and Xu, W. (2012). *Journal of Physics D: Applied Physics* 45: 11.

19 Bhattarai, J.K., Uddin Maruf, M.H., and Stine, K.J. (2020). *Processes* 8 (1): 1–20.

20 Inci, F., Saylan, Y., Kojouri, A.M. et al. (2020). *Applied Materials Today* 18: 100478.

21 Hoa, X.D., Kirk, A.G., and Tabrizian, M. (2007). *Biosensors and Bioelectronics* 23 (2): 151–160.

22 Qu, J.H., Dillen, A., Saeys, W. et al. (2020). *Analytica Chimica Acta* 1104: 10–27.

23 Mauriz, E., Dey, P., and Lechuga, L.M. (2019). *The Analyst* 144 (24): 7105–7129.

24 Zayats, A.V., Smolyaninov, I.I., and Maradudin, A.A. (2005). *Physics Reports* 408 (3–4): 131–314.

25 Petryayeva, E. and Krull, U.J. (2011). *Analytica Chimica Acta* 706 (1): 8–24.

26 Sepúlveda, B., Angelomé, P.C., Lechuga, L.M., and Liz-Marzán, L.M. (2009). *Nano Today* 4 (3): 244–251.

27 Liu, P., Wang, H., Li, X. et al. (2015). *RSC Advances* 5 (97): 79738–79745.

28 Zoric, I., Zach, M., Kasemo, B., and Langhammer, C. (2011). *ACS Nano* 5 (4): 2535–2546.

29 Wang, B., Singh, S.C., Lu, H., and Guo, C. (2020). *Plasmonics* 15 (3): 609–621.

30 Unser, S., Bruzas, I., He, J., and Sagle, L. (2015). *Sensors* 15 (7): 15684–15716.

31 Cao, J., Sun, T., and Grattan, K.T.V. (2014). *Sensors and Actuators B: Chemical* 195: 332–351.

32 Li, Z., Leustean, L., Inci, F. et al. (2019). *Biotechnology Advances* 37: 8, 107440.

33 Inci, F., Filippini, C., Baday, M. et al. (2015). *Proceedings of the National Academy of Sciences* 112 (32): E4354–E4363.

34 Inci, F., Karaaslan, M.G., Mataji-Kojouri, A. et al. (2020). *Applied Materials Today* 20: 100709.

35 Wang, Y., Zhou, J., and Li, J. (2017). *Small Methods* 1 (11): 1700197.

36 Sun, L.L., Leo, Y.S., Zhou, X. et al. (2020). *Materials Science for Energy Technologies* 3: 274–281.

37 Jatschka, J., Dathe, A., Csáki, A. et al. (2016). *Sensing and Bio-Sensing Research* 7: 62–70.

38 Acimovic, S.S., Ortega, M.A., Sanz, V. et al. (2014). *Nano Letters* 14 (5): 2636–2641.

39 Thakur, A., Qiu, G., Siu-Pang, N.G. et al. (2017). *Biosensors and Bioelectronics* 94: 400–407.

40 Qiu, G., Gai, Z., Tao, Y. et al. (2020). *ACS Nano* 14 (5): 5268–5277.

41 Rostron, P., Gaber, S., and Gaber, D. (2016). *Laser* 21: 24.

42 Wang, C., Zeng, L., Li, Z., and Li, D. (2017). *Journal of Raman Spectroscopy* 48 (8): 1040–1055.

43 Butler, H.J., Ashton, L., Bird, B. et al. (2016). *Nature Protocols* 11 (4): 664–687.

44 Haddad, A., Green, O., and Lombardi, J.R. (2019). *Spectroscopy Letters* 52 (8): 462–472.

45 Zhao, H., Hasi, W., Bao, L. et al. (2017). *Chinese Journal of Chemistry* 35 (10): 1522–1528.

46 de Oliveira Penido, C.A.F., Pacheco, M.T.T., Lednev, I.K., and Silveira, L. Jr. (2016). *Journal of Raman Spectroscopy* 47 (1): 28–38.

47 Liu, D., Wan, J., Liu, Z. et al. (2020). *Lasers in Medical Science*: 1–8.

48 Yang, S., Chen, Q., Shi, M. et al. (2020). *Nanomaterials* 10 (4): 770.

49 Bai, S., Serien, D., Hu, A., and Sugioka, K. (2018). *Advanced Functional Materials* 28: 23, 1706262.

50 Hu, G., Xiong, W., Luo, H. et al. (2018). *Applied Spectroscopy* 72 (1): 151–158.

51 Wiktelius, D., Ahlinder, L., Larsson, A. et al. (2018). *Talanta* 186: 622–627.

52 Tyndall, N.F., Stievater, T.H., Kozak, D.A. et al. (2018). *Optics Letters* 43 (19): 4803–4806.

53 Pearman, W.F. and Fountain, A.W. (2006). *Applied Spectroscopy* 60 (4): 356–365.

54 Yan, F. and Vo-Dinh, T. (2007). *Sensors and Actuators B: Chemical* 121 (1): 61–66.

55 Sinjab, F., Kong, K., Gibson, G. et al. (2016). *Biomedical Optics Express* 7 (8): 2993–3006.

56 Lin, K., Zheng, W., Lim, C.M., and Huang, Z. (2017). *Theranostics* 7 (14): 3517.

57 Haifler, M., Pence, I., Sun, Y. et al. (2018). *Journal of Biophotonics* 11: 6, e201700188.

58 Chen, H., Li, X., Broderick, N. et al. (2018). *Journal of Biophotonics* 11: 9, e201800016.

59 Farhane, Z., Bonnier, F., and Byrne, H.J. (2018). *Journal of Biophotonics* 11: 1, e201700112.

60 Zhang, H., Xiao, L., Li, Q. et al. (2018). *Biomicrofluidics* 12: 2, 24119.

61 da Silva, E.C.O., dos Santos, F.M., Ribeiro, A.R.B. et al. (2019). *The Analyst* 144 (5): 1622–1631.

62 Byrne, H.J., Bonnier, F., and Farhane, Z. (2019). *Journal of Biophotonics* 12: 3, e201800328.

63 Moore, T.J., Moody, A.S., Payne, T.D. et al. (2018). *Biosensors* 8 (2): 46.

64 Lee, M., Oh, K., Choi, H.-K. et al. (2018). *ACS Sensors* 3 (1): 151–159.

65 Song, C.Y., Yang, Y.J., Yang, B.Y. et al. (2016). *Nanoscale* 8 (39): 17365–17373.

66 Zheng, J. and He, L. (2014). *Comprehensive Reviews in Food Science and Food Safety* 13 (3): 317–328.

67 Li, C., Liu, Y., Zhou, X., and Wang, Y. (2020). *Journal of Materials Chemistry B* 8 (16): 3582–3589.

68 Sun, Y. and Li, T. (2018). *Analytical Chemistry* 90 (19): 11614–11621.

69 Zhang, X., Liu, S., Song, X. et al. (2019). *ACS Sensors* 4 (8): 2140–2149.

70 Kim, E., Baaske, M.D., and Vollmer, F. (2017). *Lab on a Chip* 17 (7): 1190–1205.

71 Nunzi Conti, G., Berneschi, S., and Soria, S. (2016). *Biosensors* 6 (3): 28.

72 Brice, I., Grundsteins, K., Atvars, A. et al. (2020). *Sensors and Actuators B: Chemical*: 128004.

73 Huckabay, H.A., Wildgen, S.M., and Dunn, R.C. (2013). *Biosensors and Bioelectronics* 45: 223–229.

74 Tosi, D., Poeggel, S., Iordachita, I., and Schena, E. (2018). Fiber optic sensors for biomedical applications. In: *Opto-Mechanical Fiber Optic Sensors* (ed. H. Alemohammad). Butterworth-Heinemann.

75 Tabassum, S. and Kumar, R. (2020). *Advanced Materials Technologies* 5 (5): 1900792.

76 Prakashan, V.P., George, G., Sanu, M.S. et al. (2020). *Applied Surface Science* 507: 144957.

77 Lu, Y., Li, H., Qian, X. et al. (2020). *Optical Fiber Technology* 56: 102187.

78 Shah, K., Sharma, N.K., and Sajal, V. (2018). *Optical and Quantum Electronics* 50 (6): 265.

79 Esposito, F., Sansone, L., Taddei, C. et al. (2018). *Sensors and Actuators B: Chemical* 274: 517–526.

80 Hromadka, J., Tokay, B., Correia, R. et al. (2018). *Sensors and Actuators B: Chemical* 255: 2483–2494.

81 Partridge, M., James, S.W., and Tatam, R.P. (2016). *Journal of Lightwave Technology* 34 (19): 4506–4510.

82 Kaushik, S., Pandey, A., Tiwari, U.K., and Sinha, R.K. (2018). *Optical Fiber Technology* 46: 95–103.

83 Kant, R. and Gupta, B.D. (2018). *Journal of Lightwave Technology* 36 (18): 4018–4024.

84 Zhou, L., Liu, C., Sun, Z. et al. (2019). *Biosensors and Bioelectronics* 137: 140–147.

85 Fajkus, M., Nedoma, J., Martinek, R. et al. (2017). *Sensors* 17 (1): 111.

86 Guner, H., Ozgur, E., Kokturk, G. et al. (2017). *Sensors and Actuators, B: Chemical* 239: 571–577.

87 Liu, Y., Liu, Q., Chen, S. et al. (2015). *Scientific Reports* 5: 1–9.

88 Yang, Q., Cai, R., Xiao, W. et al. (2018). *Nanoscale Research Letters* 13: 262.

89 Kim, S., Mitropoulos, A.N., Spitzberg, J.D. et al. (2013). *Optics Express* 21 (7): 8897.

90 Lu, T., Peng, W., Zhu, S., and Zhang, D. (2016). *Nanotechnology* 27: 050201.

91 Inan, H., Poyraz, M., Inci, F. et al. (2017). *Chemical Society Reviews* 46 (2): 366–388.

92 Sukhoivanov, I.A. and Gurvey, I.V. (2009). *Photonic Crystals: Physics and Practical Modeling*. Springer.

93 Lin, D., Tao, H., Trevino, J. et al. (2012). *Advanced Materials* 24 (45): 6088–6093.

94 Kim, S., Mitropoulos, A.N., Spitzberg, J.D. et al. (2012). *Nature Photonics* 6 (12): 818–823.

95 Che, C., Li, N., Long, K.D. et al. (2019). *Lab on a Chip* 19 (23): 3943–3953.

96 Belushkin, A., Yesilkoy, F., and Altug, H. (2018). *ACS Nano* 12 (5): 4453–4461.

97 Canovi, M., Lucchetti, J., Stravalaci, M. et al. (2012). *Sensors (Switzerland)* 12 (12): 16420–16432.

98 Park, J.E., Kim, M., Hwang, J.H., and Nam, J.M. (2017). *Small Methods* 1: 3.

99 Luan, J., Morrissey, J.J., Wang, Z. et al. (2018). *Light: Science and Applications* 7: 1.

100 Choi, B., Dou, X., Fang, Y. et al. (2016). *Physical Chemistry Chemical Physics* 18 (37): 26078–26087.

101 Radu, A.I., Ussembayev, Y.Y., Jahn, M. et al. (2016). *RSC Advances* 6 (50): 44163–44169.

102 Mataji-Kojouri, A., Ozen, M.O., Shahabadi, M. et al. (2020). *ACS Nano* 14: 8518–8527.

103 Ahmed, R., Ozen, M.O., Karaaslan, M.G. et al. (2020). *Advanced Materials* 32 (19): 1–11.

104 Shende, P., Prabhakar, B., and Patil, A. (2019). *TrAC, Trends in Analytical Chemistry* 121: 115687.

105 A. Piriya, V.S., Joseph, P., K. Daniel, S.C.G. et al. (2017). *Materials Science and Engineering: C* 78: 1231–1245.

106 Liu, D., Fang, L., Zhou, F. et al. (2018). *Advanced Functional Materials* 28: 18, 1707392.

107 Purohit, B., Kumar, A., Mahato, K., and Chandra, P. (2020). *Current Opinion in Biomedical Engineering* 13: 42–50.

108 Carrell, C., Kava, A., Nguyen, M. et al. (2019). *Microelectronic Engineering* 206: 45–54.

109 Nguyen, V.-T., Song, S., Park, S., and Joo, C. (2020). *Biosensors and Bioelectronics* 152: 112015.

110 Dalirirad, S. and Steckl, A.J. (2019). *Sensors and Actuators B: Chemical* 283: 79–86.

111 Liu, J., Ji, D., Meng, H. et al. (2018). *Sensors and Actuators B: Chemical* 262: 486–492.

112 Liang, L., Su, M., Li, L. et al. (2016). *Sensors and Actuators B: Chemical* 229: 347–354.

113 Guo, L., Jackman, J.A., Yang, H.H. et al. (2015). *Nano Today* 10 (2): 213–239.